3D MODELING OF NON-LINEAR LASER PLASMA INTERACTION IN HYDRODYNAMIC CODES - APPLICATION TO STUDY OF LOW MODES IN DIRECT-DRIVE IMPLOSIONS

FORUM ILP

SEP 29TH, 2021

A. COLAITIS[1], I. IGUMENSHCHEV[2], D. EDGELL[2], D. FROULA[2], D. TURNBULL[2], R. SHAH[2], J. PALASTRO[2], R. FOLLETT[2], O. MANION[2], C. STOECKL[2], D. JACOB-PERKINS[2], V. GONCHAROV[2]

1. CELIA, BORDEAUX
2. LLE, ROCHESTER NY

1- Introduction to inertial confinement fusion and a few typical degradation sources in implosions

2- Laser plasma transport and interaction modeling for study of low-mode degradations

3- Application to a study of “best-setup” OMEGA implosions

1- Introduction to inertial confinement fusion and a few typical degradation sources in implosions

2- Laser plasma transport and interaction modeling for study of low-mode degradations

3- Application to a study of “best-setup” OMEGA implosions

1.1 NUCLEAR FUSION REACTIONS

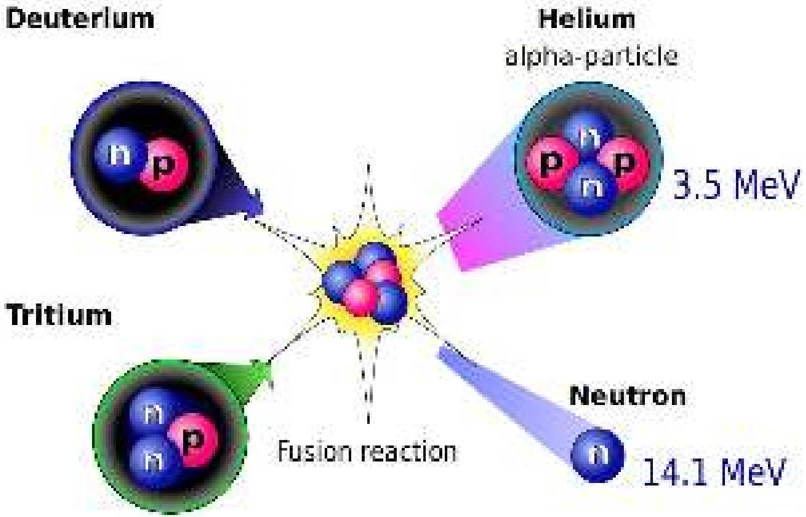

Energy density

Fusion : 339 million MJ/kg

Chemical oxydation of hydrogen : 120 MJ/kg

Combustion of TNT : 4.6 MJ/kg

1.1 NUCLEAR FUSION REACTIONS

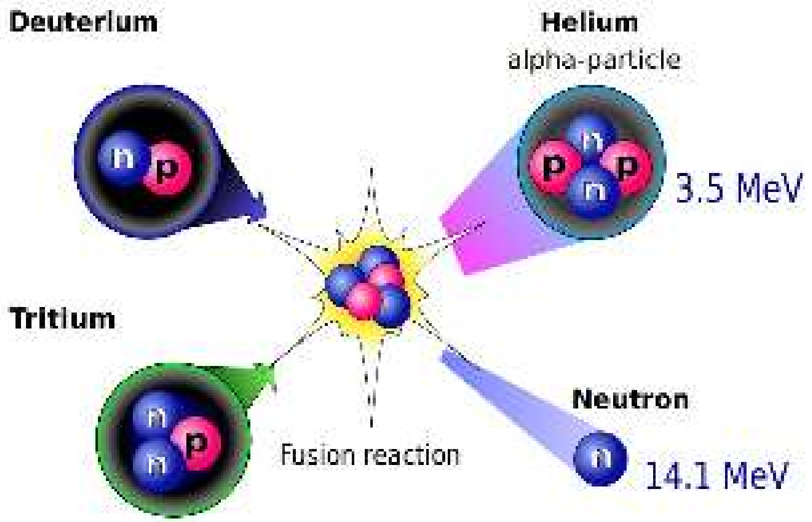

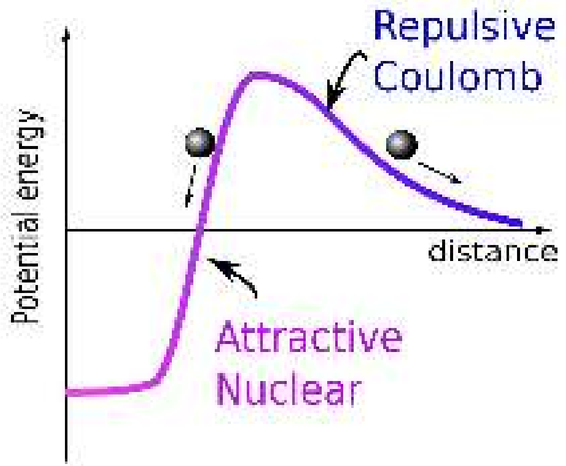

Overcoming the coulomb barrier can be achieved through the thermal motions of particules (i.e. thermonuclear fusion). The thermal approach is favored for energy production.

1.2 IGNITION OF FUSION REACTIONS

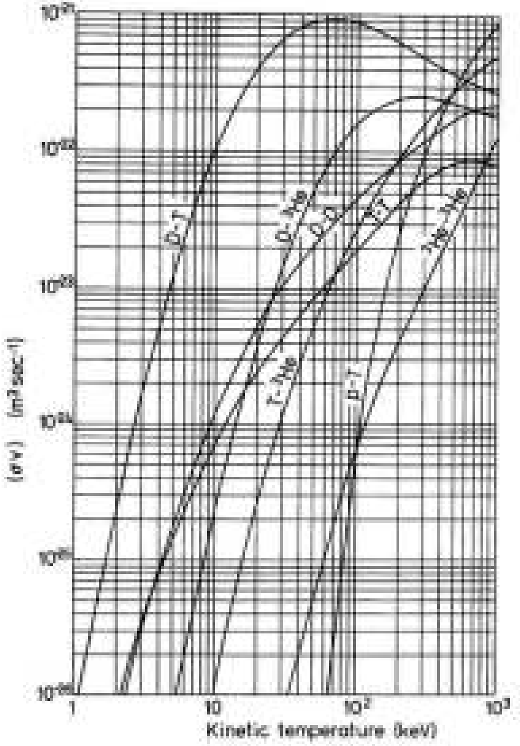

The choice of D-T as a fuel is conditionned by the reactivity (reaction probability per unit time and density)

What we need to produce significant amount of fusion reactions:

- High temperatures
- High densities

$\Longrightarrow$ high pressures

- Confinement - time for the reactions to occur to provide energy gain

Magnetic confinement: large confinement time, low density plasma - steady burn of DT fuel, continus injection of reaction mass

Inertial confinement (ICF): high density and short confinement time; targets ignited one by one

ICF: ignition condition is pressure.R >1.5 GBar.cm

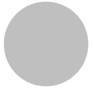

e.g. 50 microns diameter, 600 GBar

1.3 INERTIAL CONFINEMENT FUSION

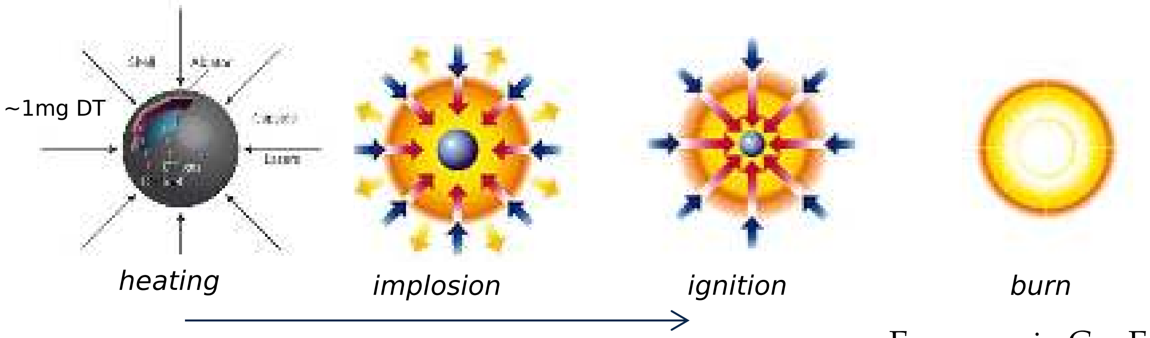

Energy gain G = Efusion/Edriver

- Compress by x1000
- Heat to 4.5 keV (~ 5 M degrees C)

⟹ Driver energy ~ 1-10 MJ in 10 ns timescale
⟹ Large scale laser facilities capables of delivering ~ 100 TW laser power are required

1.3 INERTIAL CONFINEMENT FUSION

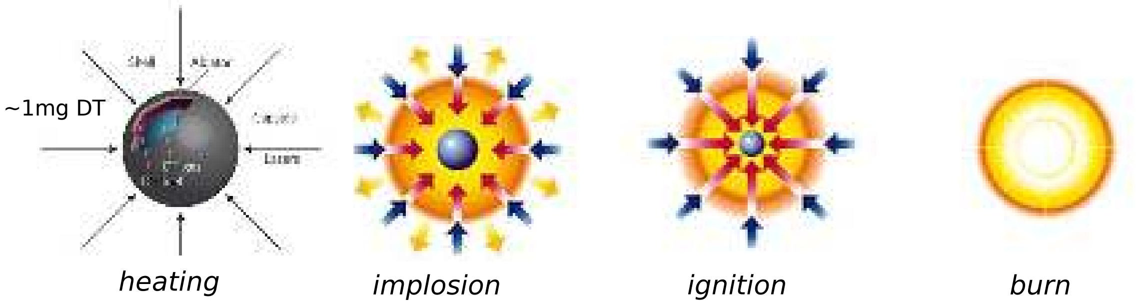

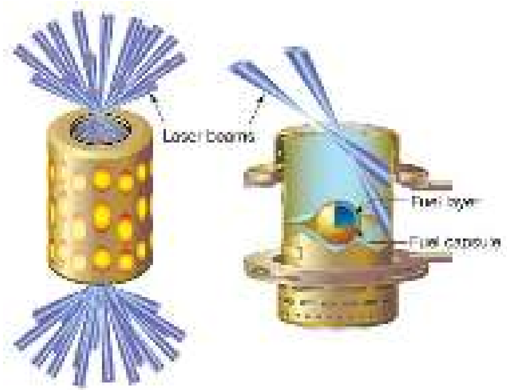

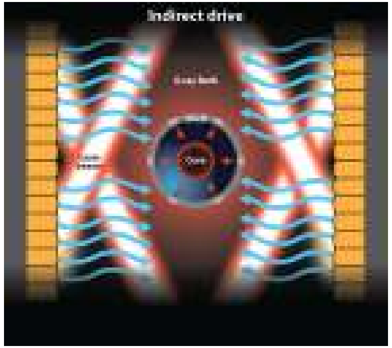

Indirect-drive approach
- Lower gain (X-ray conversion)
- Higher drive smoothness
- Time-dependant cylindrical drive to implode a spherical capsule

Direct-drive approach
- Higher gain
- More sensitive to 3D laser effects (imbalance, alignment, etc) and beam smoothness

1.3 INERTIAL CONFINEMENT FUSION

Laser MegaJoule (LMJ) - CEA CESTA

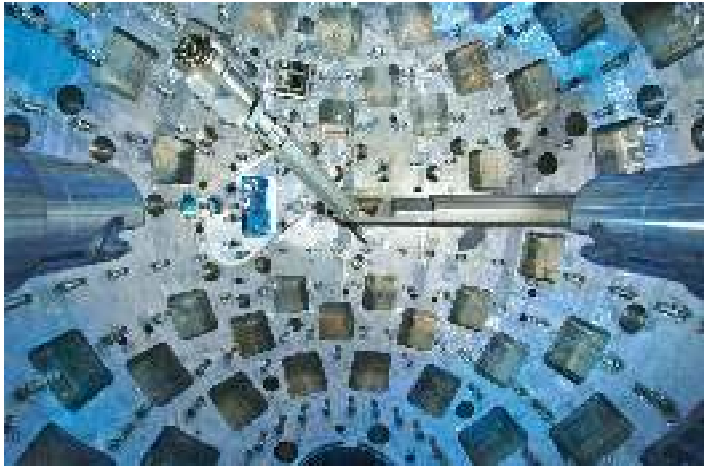

Experimental chamber (LMJ)

(full-scale, indirect-drive)

1.3 INERTIAL CONFINEMENT FUSION

NIF experimental chamber

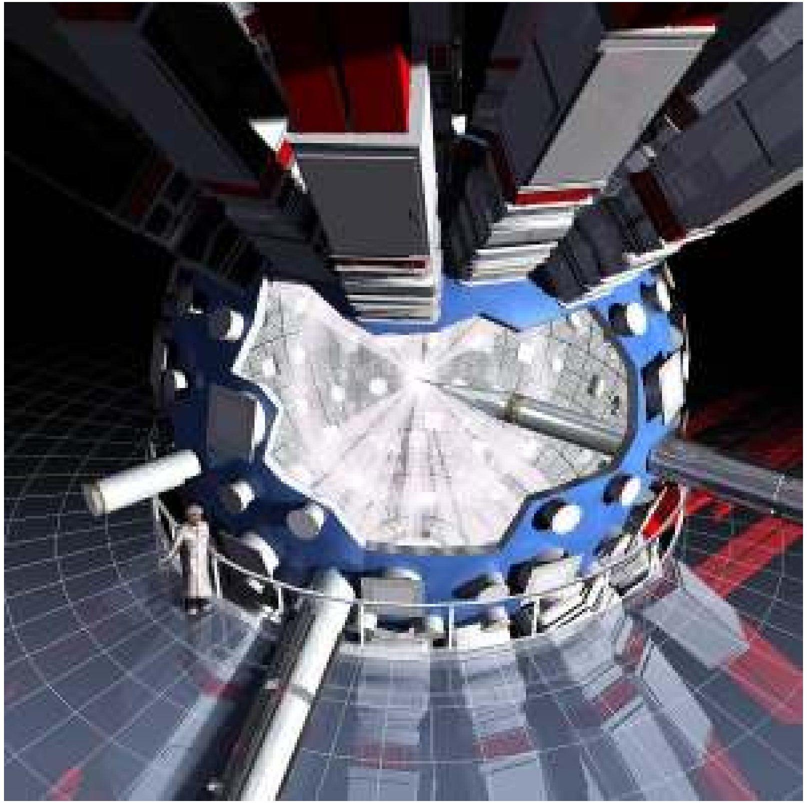

Illustration of the NIF experimental chamber and beams

(full-scale, indirect-drive)

NIF facility schematic

1.3 INERTIAL CONFINEMENT FUSION


OMEGA60 experimental chamber

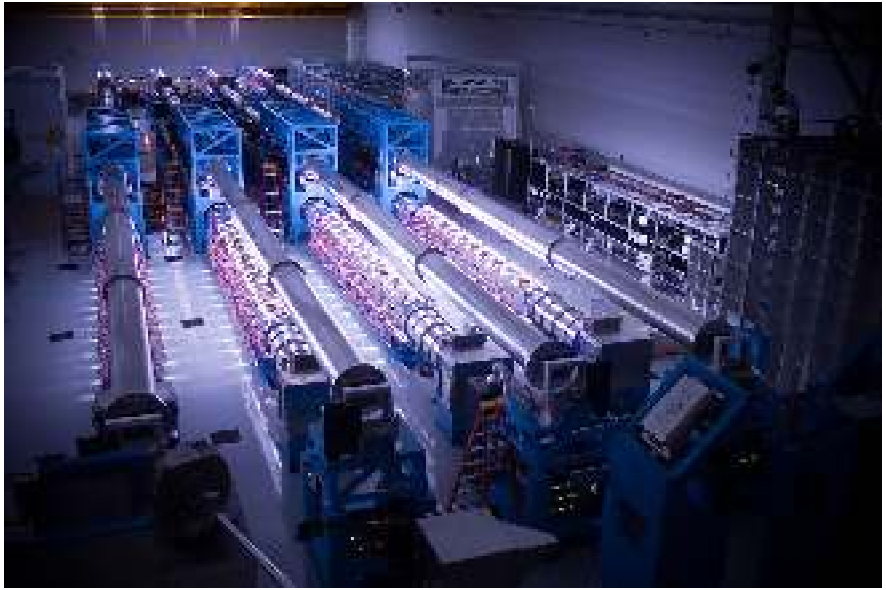
OMEGA60 amplifiers

(sub-scale, direct-drive)

1.4 TARGET IMPLOSION AND IGNITION

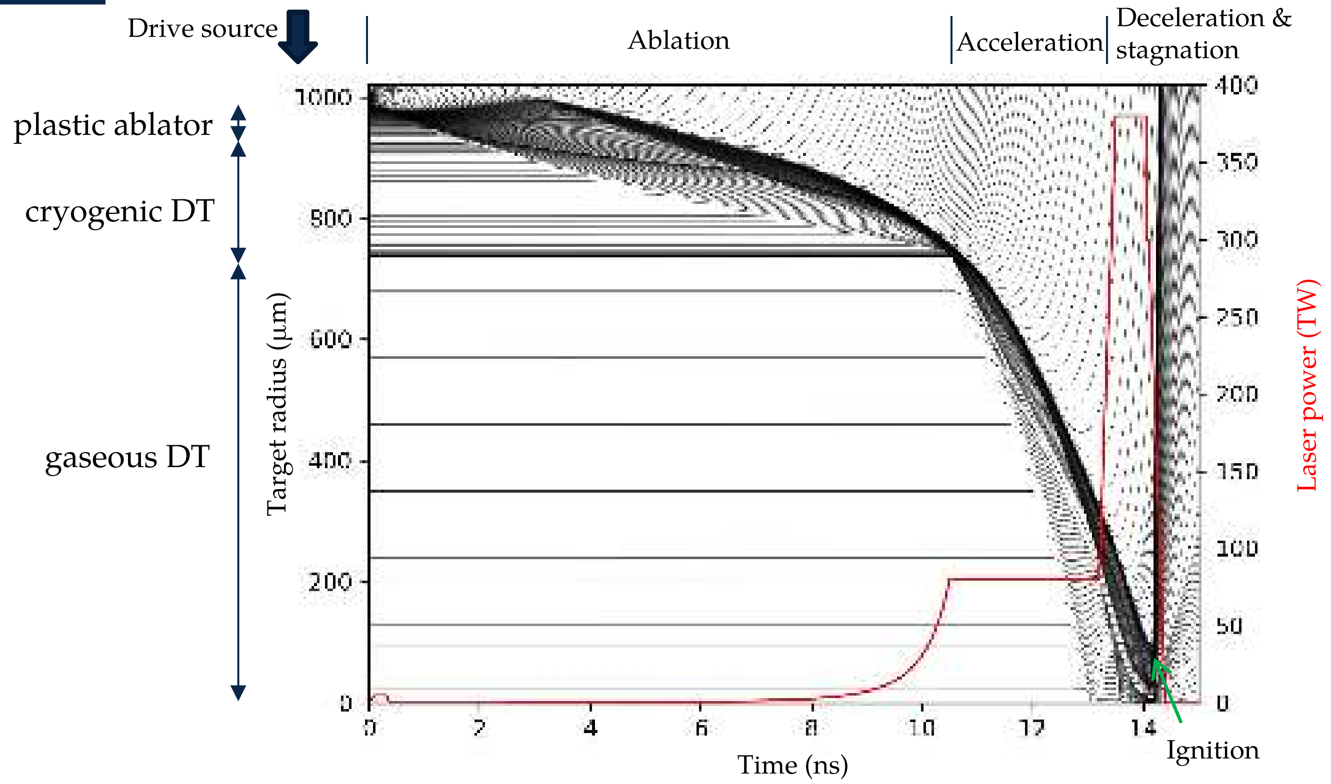

Example here is direct-drive shock ignition
There are several direct-drive ignition schemes considered: central hot-spot ignition ignition, fast ignition, shock ignition, dynamic shell, etc...

1.5 RECENT RESULTS BROUGHT THE BEST PERFORMER AT G~0.7 IN INDIRECT-DRIVE

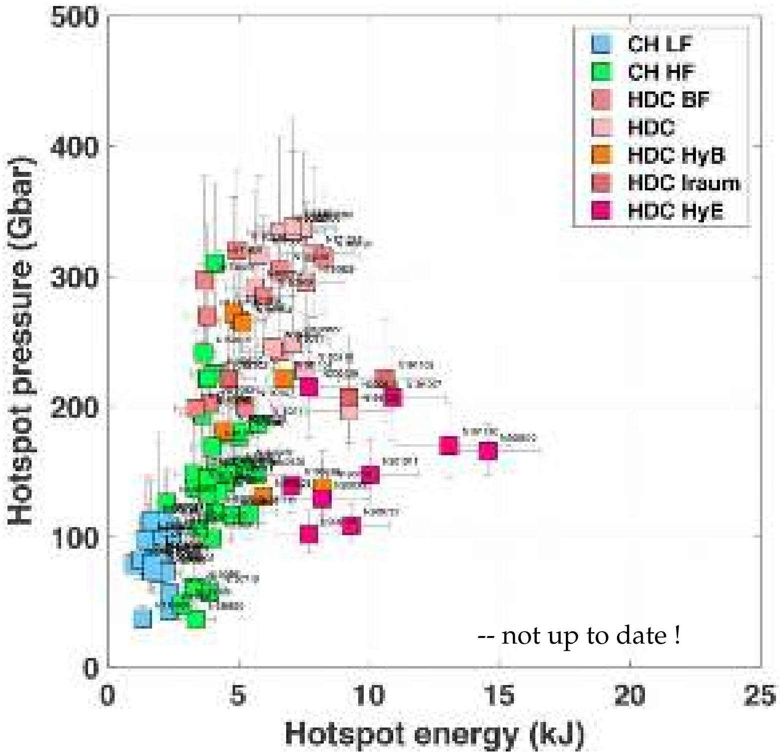

Current record:
1.3 MJ yield for ~ 1.9 MJ laser energy => G~0.7
~ 230 kJ was coupled to the spherical target
~ 12 kJ was coupled to the hotspot
~ 15 PW of fusion power for ~90 ps
~ Hotspot ion temperature of about 11 keV

Factors several key improvments; including:

- better than usual HDC layer quality (holes and angular uniformity)
- good laser delivery (but still ~ 3% imbalance)
- small fill tube (2 microns thickness)
- ...

NIF is likely to reach ignition in the coming months/years. However, high gain cannot be obtained in indirect-drive due to the Holhraum intermediary.

1.6 COMMON SOURCES OF YIELD DEGRADATION

⟹ Laser-Plasma coupling instabilities

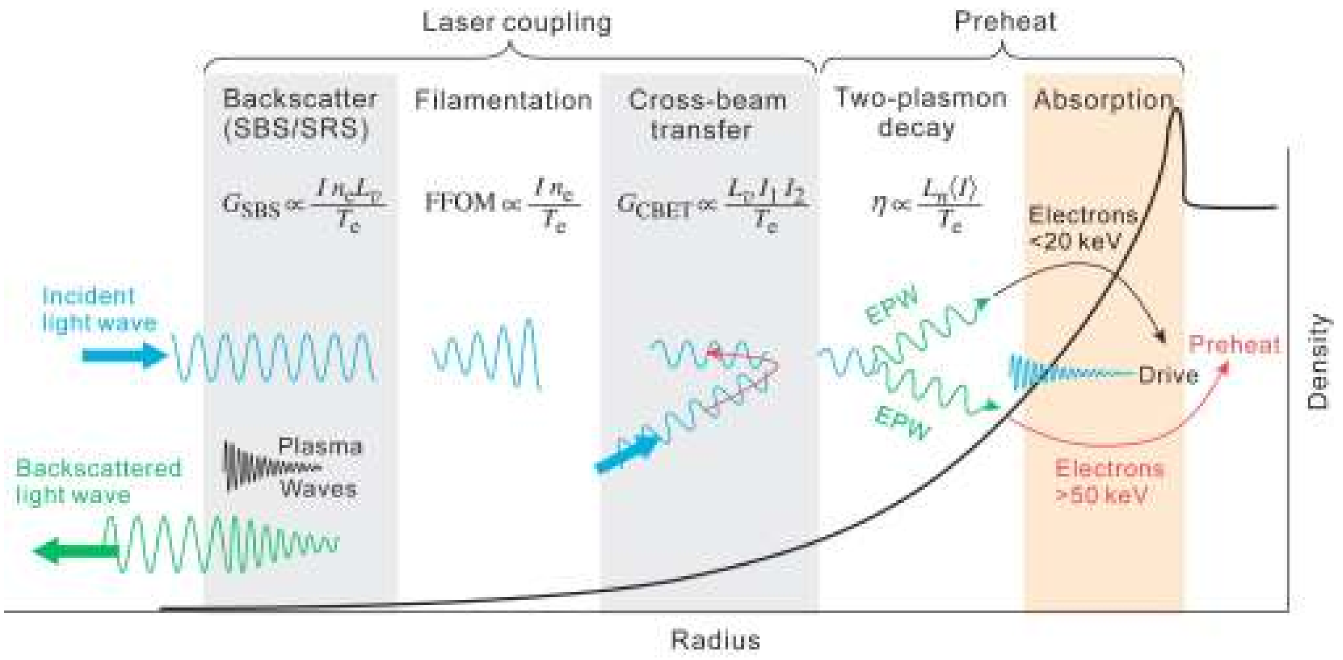

[Campbell et al., MRE (2017)]

1.6 COMMON SOURCES OF YIELD DEGRADATION

⟹ Hydrodynamic instabilities (high modes)

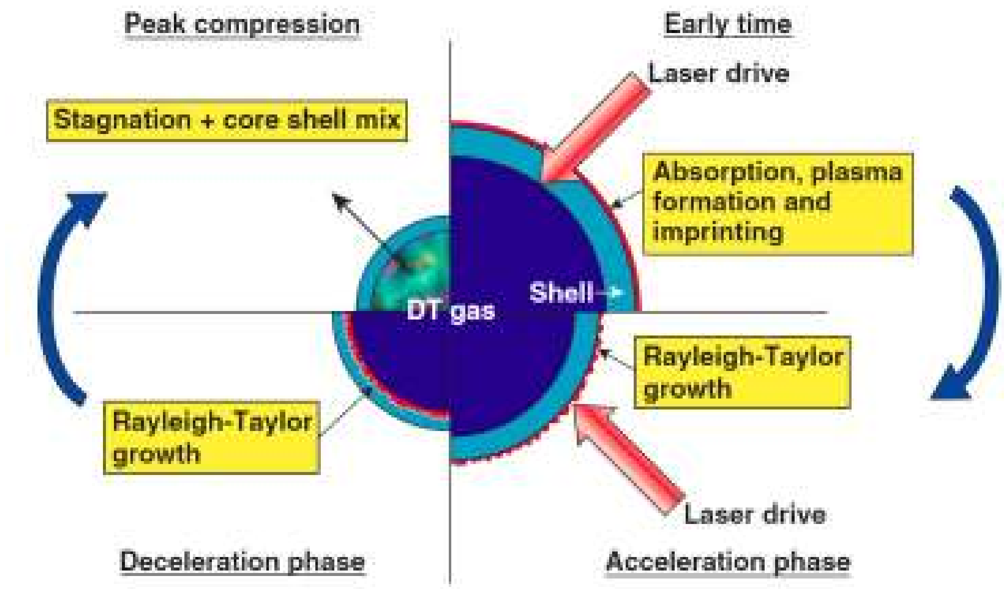

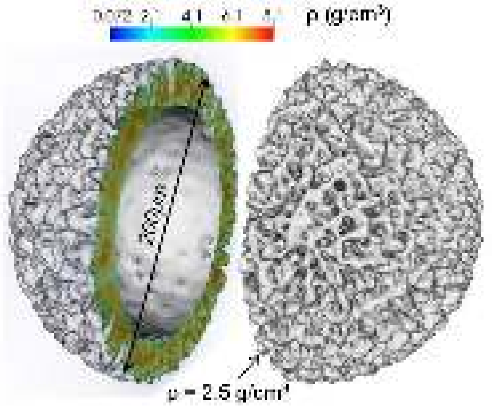

[I. V. Igumenshchev, LLE Report]

[Campbell et al., IAEA (2018)]

1.6 COMMON SOURCES OF YIELD DEGRADATION

⟹ Low modes

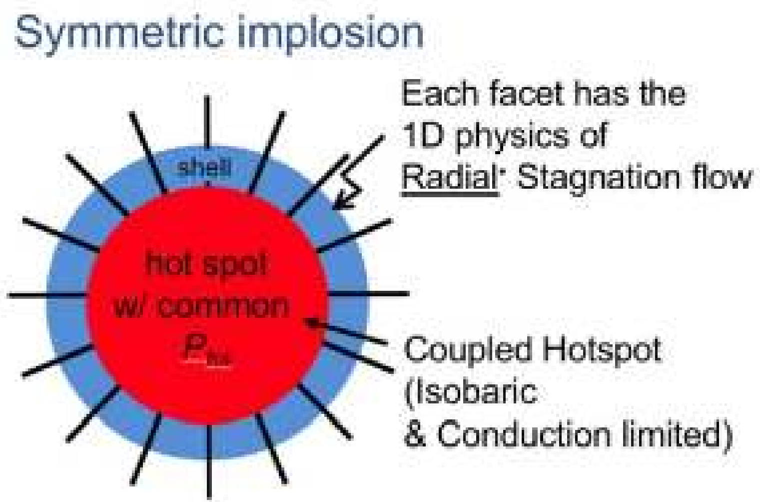

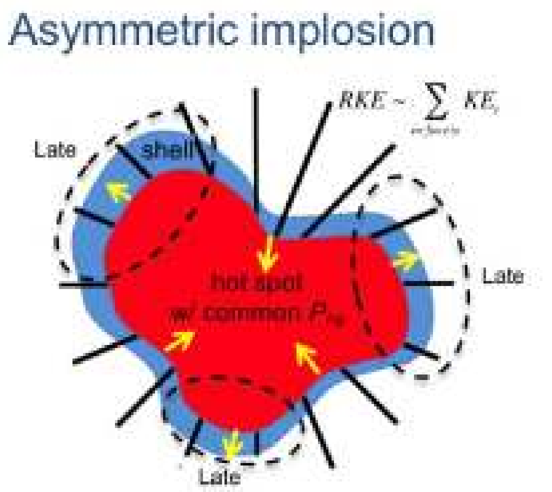

... in the rest of this talk, we will look at low mode flow anomalies in current OMEGA experiments, and discuss modeling capabilities developped in that framework at CELIA

[P. T. Springer et al. Nucl. Fus. (2019)]

1.7 RECENT OMEGA EXPERIMENT EXHIBIT SYSTEMATIC FLOW ANOMALY

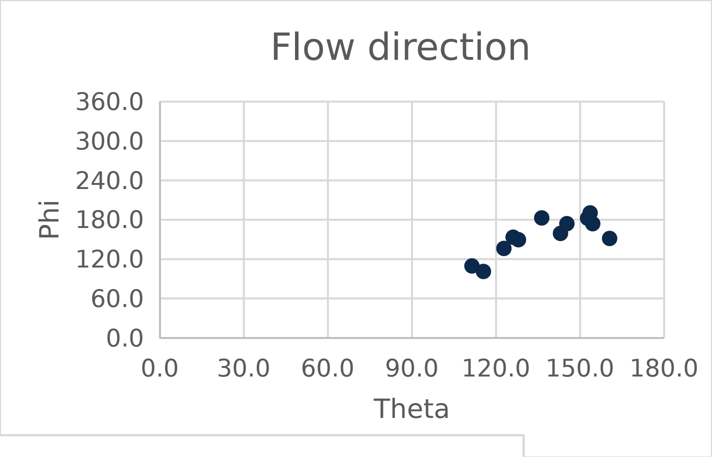

Looking at 2 years of implosions on OMEGA (2019 - 2020), and selecting only shots with:

- good ice thickness uniformity
- good ice surface roughness
- low pointing error (<2% l=1, <2% l=2 to <1% l =1)
- low power imbalance
- low target offset (< 5 microns to < 1 micron)

... there seem to remain some significant source of mode 1 assymetry that is not correlated to the mispointing

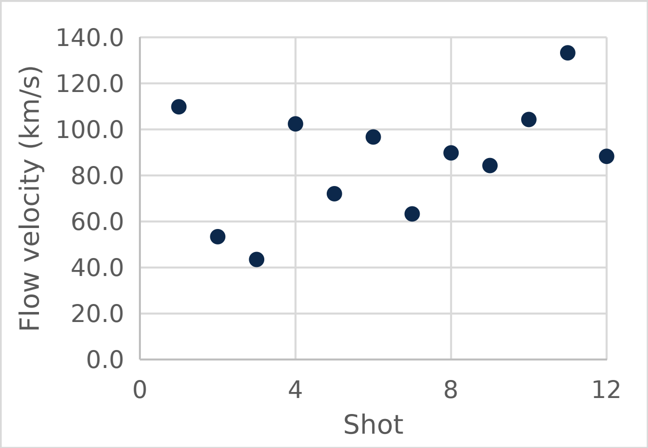

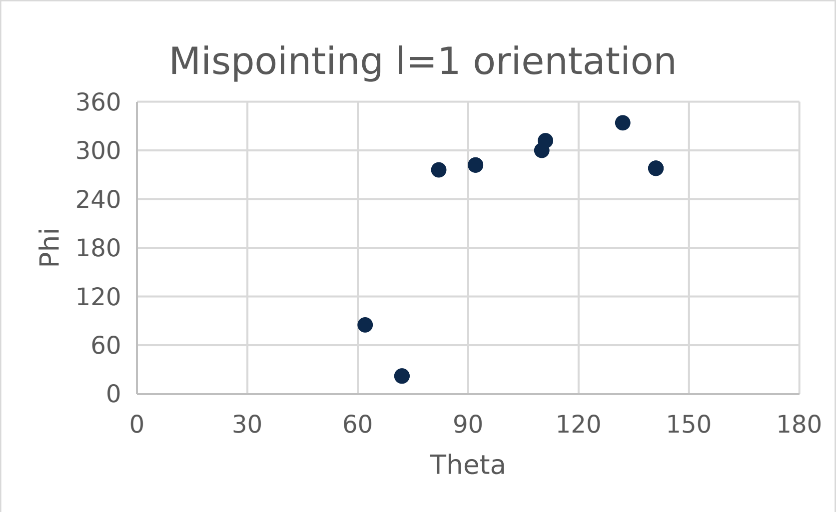

1.8 THERE ARE MANY SOURCES OF LOW MODE ASYMMETRY...

Chamber geometry

Pointing error

Beam balance

Target offset

Cross Beam Energy Transfer

Polarization effects

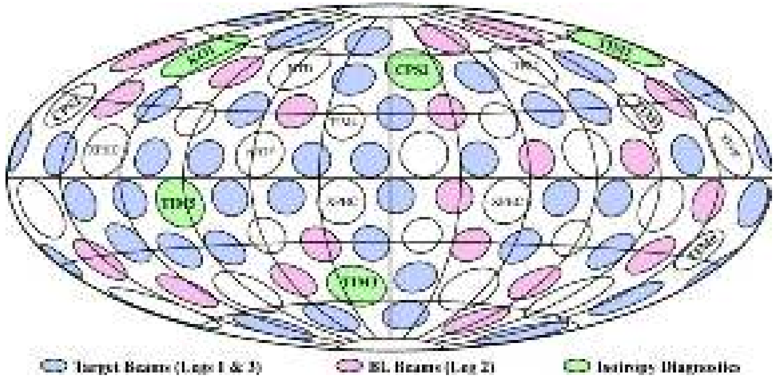

Truncated icosahedron (60 vertices) => spherical harmonics mode l=10 is strong

[M. Manuel et al. RSI 83 (2012)]
[T. R. Boehly et al. Opt Com 133 (1997)]

1.8 THERE ARE MANY SOURCES OF LOW MODE ASYMMETRY…

Chamber geometry

Pointing error

Beam balance

Target offset

Cross Beam Energy Transfer

Polarization effects

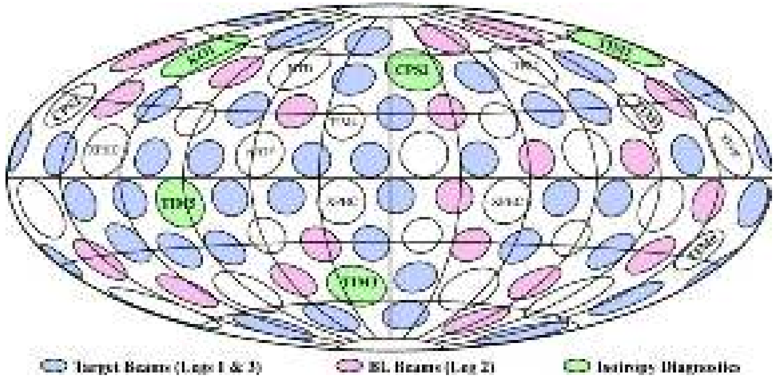

Truncated icosahedron (60 vertices) => spherical harmonics mode l=10 is strong

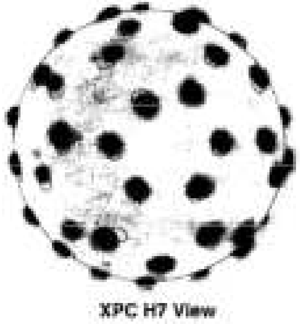

Example X-ray imaging of hard sphere illumated by 60 beams, with ideal pointing shown as circles

[M. Manuel et al. RSI 83 (2012)]
[T. R. Boehly et al. Opt Com 133 (1997)]

1.8 THERE ARE MANY SOURCES OF LOW MODE ASYMMETRY…

Chamber geometry

Pointing error

Beam balance

Target offset

Cross Beam Energy Transfer

Polarization effects

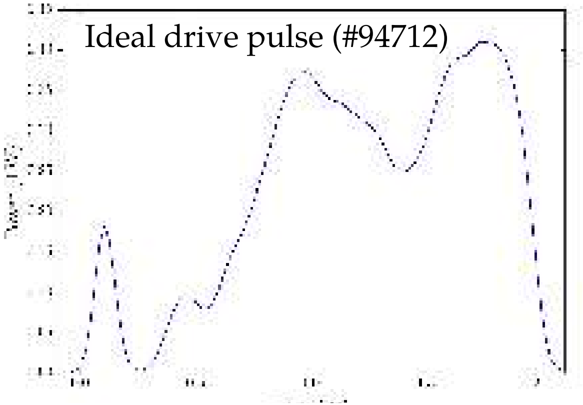

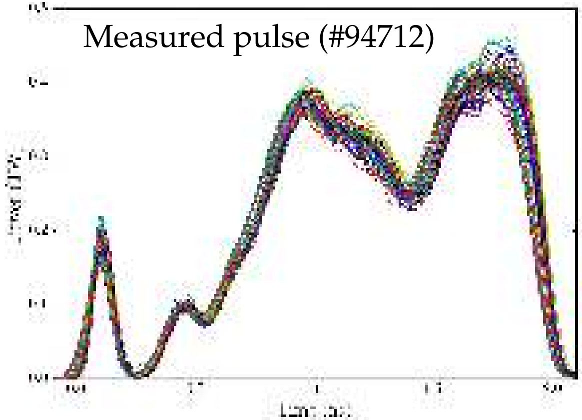

- In that case; average standard deviation of 3.3% of peak power
- Modes change dynamically during the profile !

1.8 THERE ARE MANY SOURCES OF LOW MODE ASYMMETRY…

Chamber geometry

Pointing error

Beam balance

Target offset

Cross Beam Energy Transfer

Polarization effects

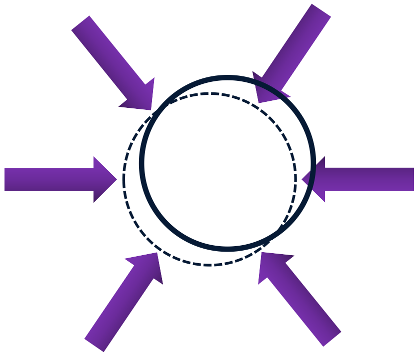

Ranging from 0 (ideal) to ~ 40 microns (bad performance)

Most likely, we need under 5 microns of accuracy (at OMEGA scale)

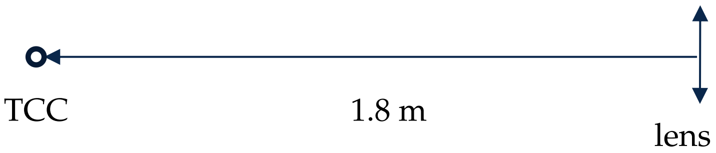

If the pointing accuracy was the size of a basketball, this would be comparable to scoring a basket from 86 km away

CROSS BEAM ENERGY TRANSFER CAN LEAD TO LARGE POWER REDISTRIBUTION BETWEEN BEAMS

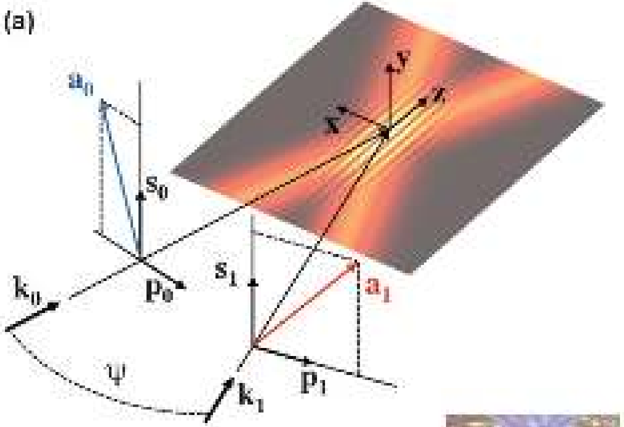

[P. Michel et al. PRL 113 (2014)]

$$2k_{1z}a_1' = -i\frac{\omega_{p0}^2}{2c^2}\frac{\delta n^*}{n_0}a_0,$$

$$2k_{0z}a_0' = -i\frac{\omega_{p0}^2}{2c^2}\frac{\delta n}{n_0}a_1,$$

The CBET interaction depends on the wavelength of the interacting beams, polarization vectors, local velocity profile, and IAW response (i.e. plasma composition and electron distribution function)

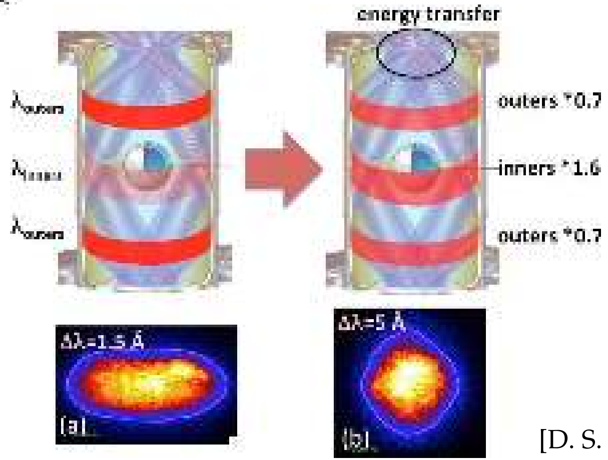

[D. S. Montgomery et al. PoP 23 (2016)]
[P. Michel et al. PoP 17 (2010)]

1.8 THERE ARE MANY SOURCES OF LOW MODE ASYMMETRY…

Chamber geometry

Pointing error

Beam balance

Target offset

Cross Beam Energy Transfer

Polarization effects

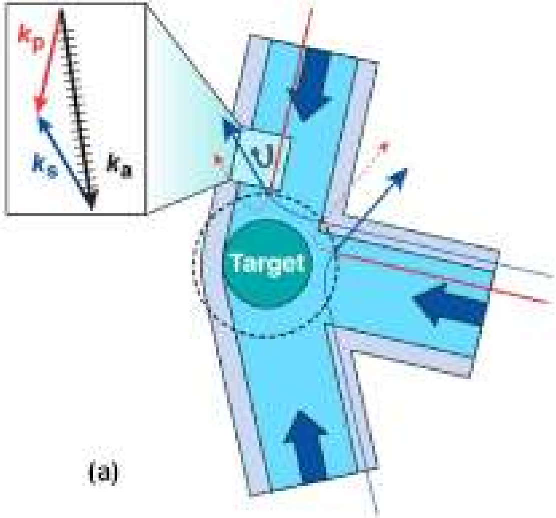

[A. K. Davis et al. PoP (2016)]

If the laser configuration is perfectly symetric, the CBET also produces symetric irradiation, just changing modes and coupling

1.8 THERE ARE MANY SOURCES OF LOW MODE ASYMMETRY...

Chamber geometry

Pointing error

Beam balance

Target offset

Cross Beam Energy Transfer

Polarization effects

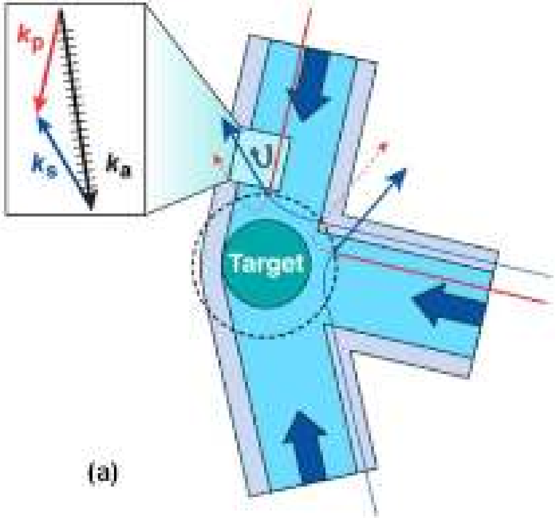

If the laser configuration is perfectly symetric, the CBET also produces symetric irradiation, just changing modes and coupling

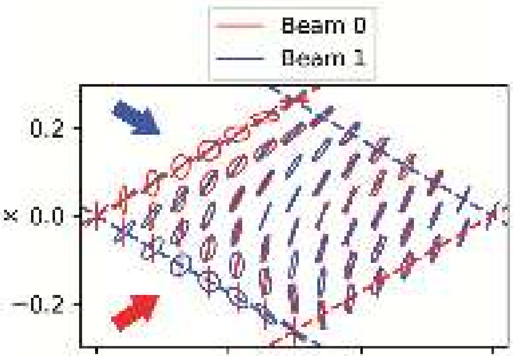

Accounting for polarization changes the CBET.

The polarized beam configuration on OMEGA is not symetric !

E. Kur et al. Optics Express 29 (2021)

1- Introduction to inertial confinement fusion and a few typical degradation sources in implosions

2- Laser plasma transport and interaction modeling for study of low-mode degradations

3- Application to a study of “best-setup” OMEGA implosions

2.1 MODELING LASER PROPAGATION IN PLASMAS; A NAIVE APPROACH

Time envelopped wave equation for the electric field of a transverse wave in plasma:

$$\frac{2i\omega_0}{c^2}\frac{\partial}{\partial t}\mathbf{E} + \nabla^2\mathbf{E} - \nabla(\nabla\cdot\mathbf{E}) + \frac{\omega_0^2}{c^2}\epsilon(\omega_0;\mathbf{x},t)\mathbf{E} = 0,$$

Here one must resolve the wave frequency (e.g. 351 nm/10 cells) and the time derivative depends on numerical scheme and resolved equations beside that of light, but is of the order of 2 ps

2.1 MODELING LASER PROPAGATION IN PLASMAS; A NAIVE APPROACH

Time envelopped wave equation for the electric field of a transverse wave in plasma:

$$\frac{2i\omega_0}{c^2}\frac{\partial}{\partial t}\mathbf{E} + \nabla^2\mathbf{E} - \nabla(\nabla\cdot\mathbf{E}) + \frac{\omega_0^2}{c^2}\epsilon(\omega_0;\mathbf{x},t)\mathbf{E} = 0,$$

Here one must resolve the wave frequency (e.g. 351 nm/10 cells) and the time derivative depends on numerical scheme and resolved equations beside that of light, but is of the order of 2 ps

Implosion-scale plasma: 1 cm, 10 ns dt = 2ps, dx = 35 nm
⟹ 5M timesteps
⟹ 2D - 80G cells / 3D - 23000000G cells
... assuming you track 10 double precision numbers per cells:
⟹ RAM required; 2D - 6.5 To (doable on ~10000 cores) / 3D - 1800 Po
... and 3D effects are important ! (geometry, speckle statistics, finite-length effects, etc...)

2.1 MODELING LASER PROPAGATION IN PLASMAS; A NAIVE APPROACH

Wave equation for a monochromatic wave of frequency omega in a weakly perturbed plasma:

$$\left[\frac{\partial}{\partial t} + \mathbf{v}_g.\nabla + 2\nu^{\mathrm{EM}}_{\nu_{\mathrm{IB}}\ll\omega} - \imath\frac{c^2}{2\omega}\Delta_\perp\right] E_0 = -\imath\frac{\omega}{2n_c}\delta n E_0$$

Here one must resolve the wave frequency (e.g. 351 nm/10 cells) and the time derivative depends on numerical scheme and resolved equations beside that of light, but is of the order of 2 ps

Implosion-scale plasma: 1 cm, 10 ns dt = 2ps, dx = 35 nm
⟹ 5M timesteps
⟹ 2D - 80G cells / 3D - 23000000G cells
... assuming you track 10 double precision numbers per cells:
⟹ RAM required; 2D - 6.5 To (doable on ~10000 cores) / 3D - 1800 Po
... and 3D effects are important ! (geometry, speckle statistics, finite-length effects, etc...)

⟹ smaller size (~ 500 microns), shorter timescales (~10-100 ps)
⟹ simplify light modeling (and sacrifice some of the details of the coupling...)

2.2 GEOMETRICAL OPTICS MODELING FOR HYDRODYNAMIC SCALES

At the largest scales, the light propagation modeling is often reduced to geometrical optics:

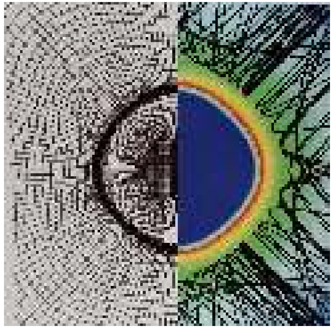

$$\frac{\mathrm{d}\mathbf{r}}{\mathrm{d}\tau} = \mathbf{p} \qquad \frac{\mathrm{d}\mathbf{p}}{\mathrm{d}\tau} = \frac{1}{2}\nabla\epsilon(\mathbf{r}) \qquad \frac{\mathrm{d}P}{\mathrm{d}\tau} = -\epsilon'' P(\mathbf{r}(\tau))$$

using just these equations; we only model collisional absorption... and thus miss a large part of the laser/plasma coupling

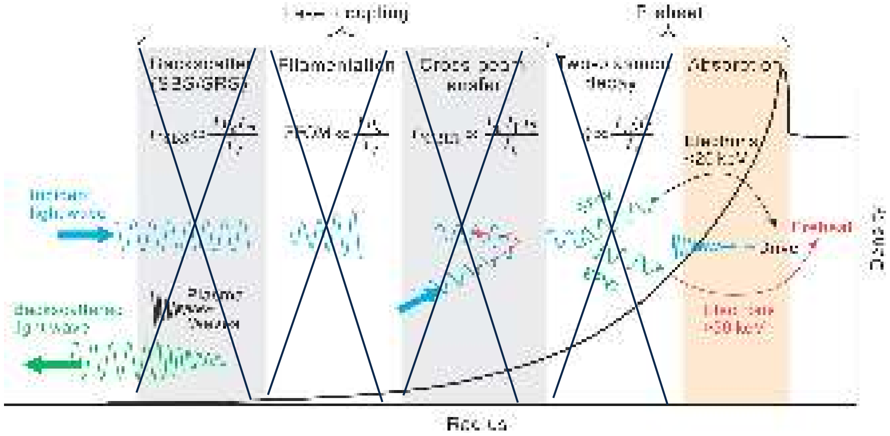

2.2 GEOMETRICAL OPTICS MODELING FOR HYDRODYNAMIC SCALES

At the largest scales, the light propagation modeling is often reduced to geometrical optics:

$$\frac{d\mathbf{r}}{d\tau} = \mathbf{p} \qquad \frac{d\mathbf{p}}{d\tau} = \frac{1}{2}\nabla\epsilon(\mathbf{r}) \qquad \frac{dP}{d\tau} = -\epsilon'' P(\mathbf{r}(\tau))$$

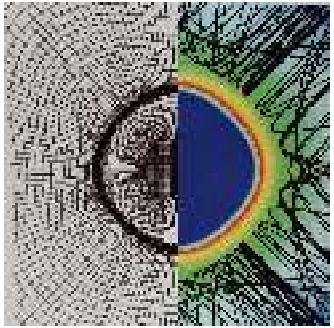

using just these equations; we only model collisional absorption... and thus miss a large part of the laser/plasma coupling

⟹ A lot of work has been carried out in developping more advanced ray-trace based models that allow to capture the finer scale physics while retaining CPU efficiency

Example shown in what follows:
3D modeling of the laser plasma interaction for collisional absorption + langdon effect + (polarized) CBET, coupled to hydrodynamics

2.2 THE RAY FIELD FORMULATION OF GEOMETRICAL OPTICS RAY TRACING

In ray optics, you can write the ray field as:

$$u(\mathbf{r}) = A_{01}(\mathbf{r}) \exp ik_0\psi_1(\mathbf{r})$$

ray field   ray amplitude   ray phase

ray phase space parameters

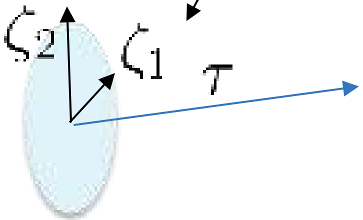

First order solution: the ray trajectory and phase

$$\Delta u(\mathbf{r}) + k_0^2\epsilon(\mathbf{r})u(\mathbf{r}) = 0$$

ray phase equation

$$(\nabla\psi)^2 = \epsilon(\mathbf{r}) \Longrightarrow \frac{d\mathbf{r}}{d\tau} = \mathbf{p} \quad \frac{d\mathbf{p}}{d\tau} = \frac{1}{2}\nabla\epsilon(\mathbf{r}) \quad \frac{d\psi}{d\tau} = \epsilon(\mathbf{r}) \quad \frac{dP}{d\tau} = -\epsilon'' P(\mathbf{r}(\tau))$$

Second order solution: the ray amplitude

$$2(\nabla A_0.\nabla\psi) + A_0\Delta\psi = 0 \Longrightarrow A_0(\tau) = A_0^0\left(\frac{D_0}{D(\tau)}\right)^{1/2}$$

ray amplitude equation

2.3 THE HYDRODYNAMICS ULTIMATELY ONLY NEEDS A LASER HEAT SOURCE TERM

Absorption is not computed along rays, but from the fields:

$$\Omega_i^{hs} = \sum_{b \in beams} \frac{m_e^2 \omega_{b,0}^3}{2e^2 \mu_0} \epsilon''_{b,i} \int_{V_i} \sum_{s \in sheets} |u_s^2| dV$$

- Methods to solve for fields are in general different than absorption along rays
- At least 5 different widespread methods to solve the absorption and fields using rays... Each has merit and shortcomings. Here we present one: Inverse Ray Tracing (IRT)
- IRT for spherical plasmas is both fast and high order in space, allowing for 3D calculations of non-linear effects at reasonable CPU costs. Implemented in the IFRIIT* inline/offline propagation code.
- Coupled to the ASTER** 3D radiation hydrodynamics code using heterogeneous parallelism on decoupled grids***

* [A. Colaïtis et al. PoP 26 (2019)]
** [I. V. Igumenshchev et al. PoP 23 (2016)]
*** see [A. Colaïtis et al. JCP (2021)] for details

2.4 A SIMPLE EXAMPLE: FIELD COMPUTATION IN A LINEAR LAYER

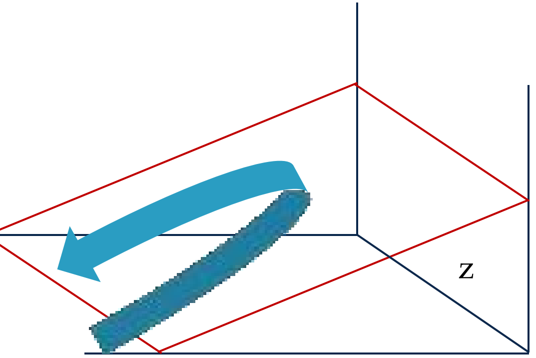

plane wave
at an angle

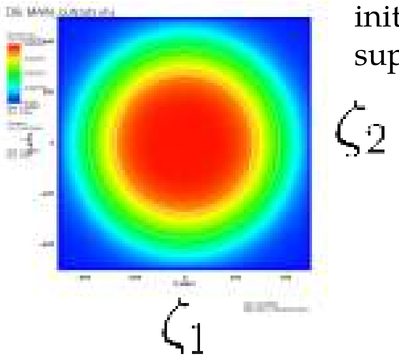

initial ray surface:
super-gaussian spot

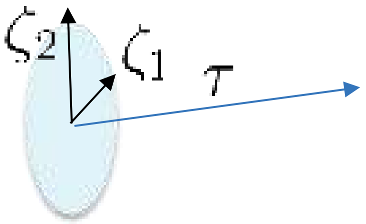

Step 1; compute the mapping from phase space (ζ_1, ζ_2) to real space (x, y)

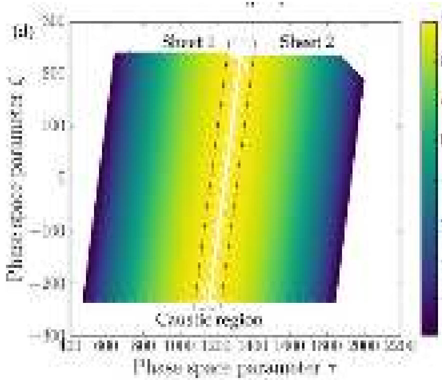

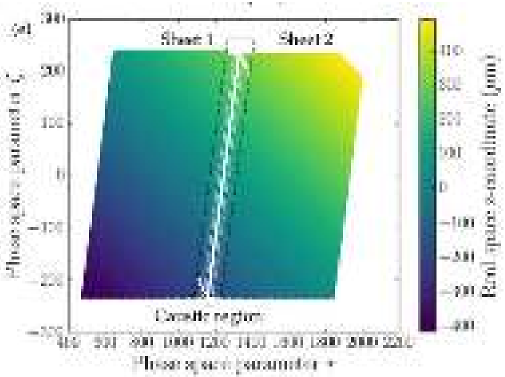

Note;
- the white “hole”... a caustic; location of ray optics inapplicatilibty !
- the two sheets

A SIMPLE EXAMPLE: FIELD COMPUTATION IN A LINEAR LAYER

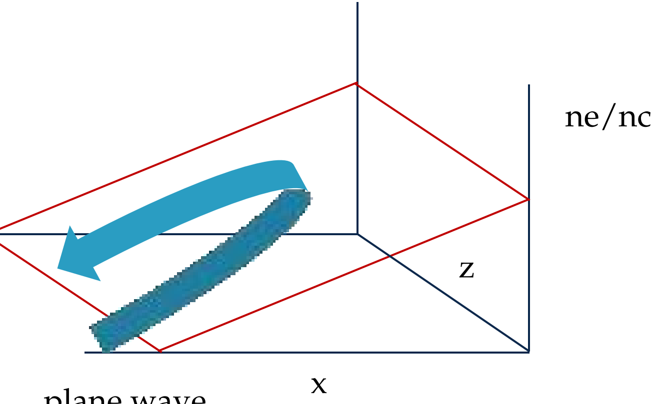

plane wave
at an angle

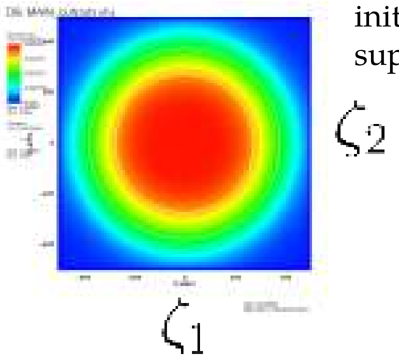

initial ray surface:
super-gaussian spot

$$\frac{d\psi}{d\tau} = \epsilon(\mathbf{r})$$

$$A_0(\tau) = A_0^0 \left(\frac{D_0}{D(\tau)} \right)^{1/2}$$

Step 2; compute the ray amplitude and phase to get the total field on each sheet

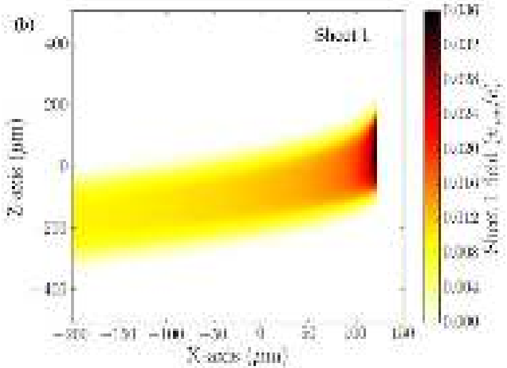

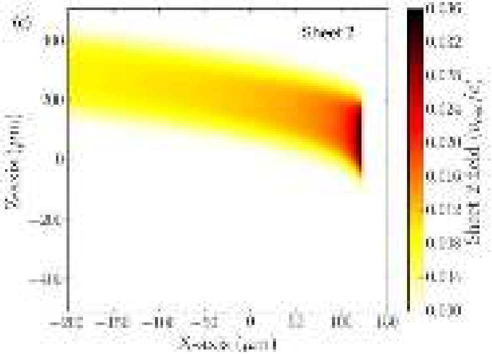

The field at caustics is reconstructed using a specific method not detailed here...

2.4 A SIMPLE EXAMPLE: FIELD COMPUTATION IN A LINEAR LAYER

Step 3; compute the total field and account for non-linear coupling effects (recall that fields/absorption depends on the permittivity)

$$\epsilon''_{i,j} = \epsilon''_{0,i} f_L + \delta\epsilon''_{i,j}$$

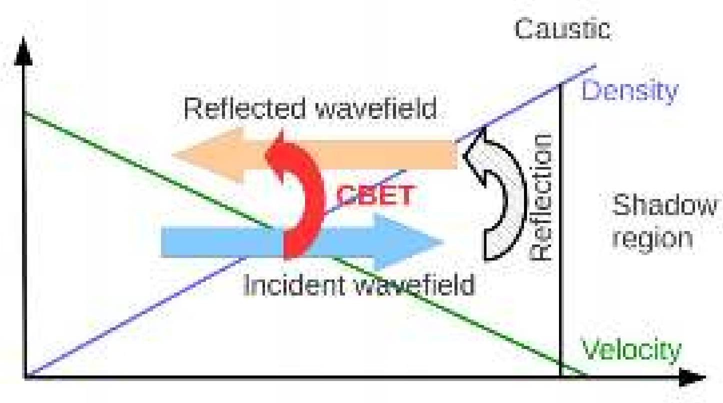

- Langdon effect: absorption depends on field due to EDF flattening

$$\alpha = \frac{Z_{\text{eff}} c^2}{v_{\text{th}}^2} \sum_{\substack{i \in \text{beams} \\ j \in \text{sheets}}} |u_{i,j}|^2 , \qquad f_L = [1 - 0.553/(1 + (0.27/\alpha)^{0.75})] .$$

- Cross-beam energy transfer: beams can transfer energy through coupling to a common ion accoustic grating created by their interaction

$$\delta\epsilon_{ij} = \frac{\chi_{i,j} c^2}{4\omega_{\text{pe}}^2} \left[\sum_{\substack{l \in \text{beams} \\ m \in \text{sheets}}} |\mathbf{k}_{ij} - \mathbf{k}_{lm}|^2 |u_{lm}|^2 K_{lm} + \sum_{\substack{m \in \text{sheets} \\ m \neq j}} |\mathbf{k}_{ij} - \mathbf{k}_{im}|^2 |u_{im}|^2 K_{im} \right]$$

2.4 A SIMPLE EXAMPLE: FIELD COMPUTATION IN A LINEAR LAYER

Step 3; compute the total field and account for non-linear coupling effects (recall that fields/absorption depends on the permittivity)

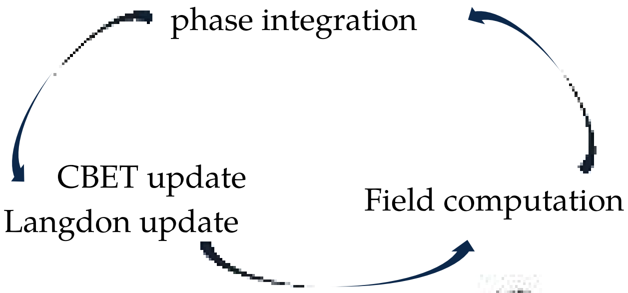

$$\epsilon''_{i,j} = \epsilon''_{0,i} f_L + \delta\epsilon''_{i,j}$$

- Langdon effect: absorption depends on field due to EDF flattening

$$\alpha = \frac{Z_{\text{eff}} c^2}{v_{\text{th}}^2} \sum_{\substack{i \in \text{beams} \\ j \in \text{sheets}}} |u_{i,j}|^2 , \qquad f_L = [1 - 0.553/(1 + (0.27/\alpha)^{0.75})] .$$

- Cross-beam energy transfer: beams can transfer energy through coupling to a common ion accoustic grating created by their interaction

$$\delta\epsilon_{ij} = \frac{\chi_{i,j} c^2}{4\omega_{pe}^2} \left[\sum_{\substack{l \in \text{beams} \\ m \in \text{sheets}}} |\mathbf{k}_{ij} - \mathbf{k}_{lm}|^2 |u_{lm}|^2 K_{lm} + \sum_{\substack{m \in \text{sheets} \\ m \neq j}} |\mathbf{k}_{ij} - \mathbf{k}_{im}|^2 |u_{im}|^2 K_{im} \right]$$

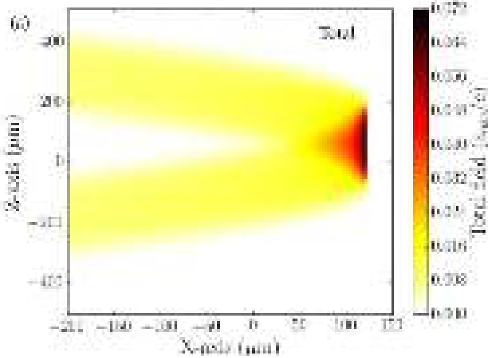

Step 4: compute absorption from converged fields

2.5 WHAT RAY PHASE SPACE LOOKS LIKE IN SPHERICAL GEOMETRY

Mapping of tau (~ ray propagation time) to real space

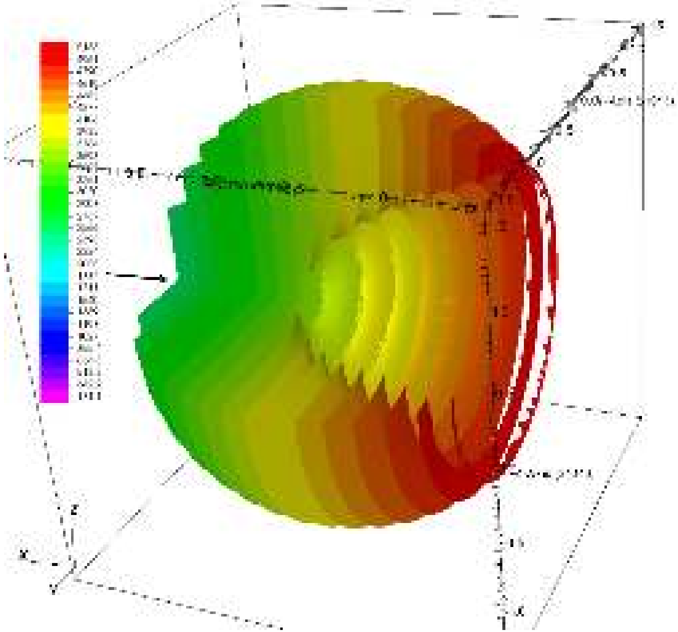

Sheet 1 (incident field)

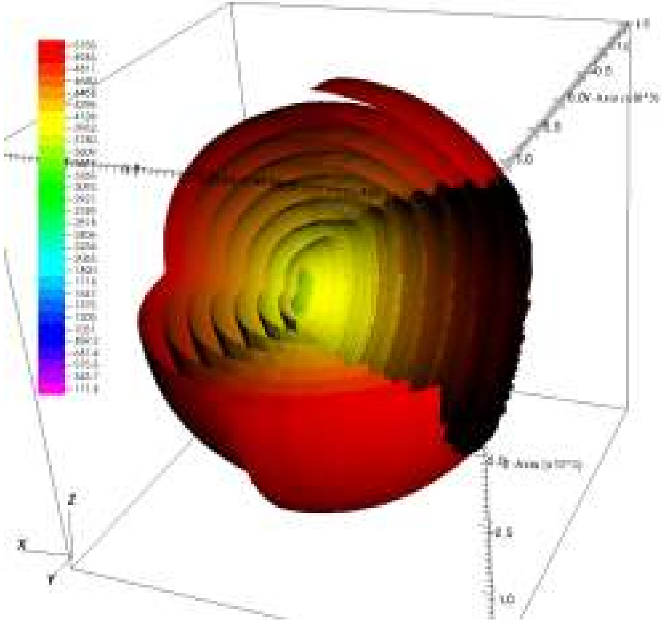

Sheet 2 (reflected field)

2.6 THE CBET IS DIRECT-DRIVE SPHERICAL GEOMETRY IS A CHALLENGING CALCULATION

The CBET interaction in direct-drive couples many beams because of overlap

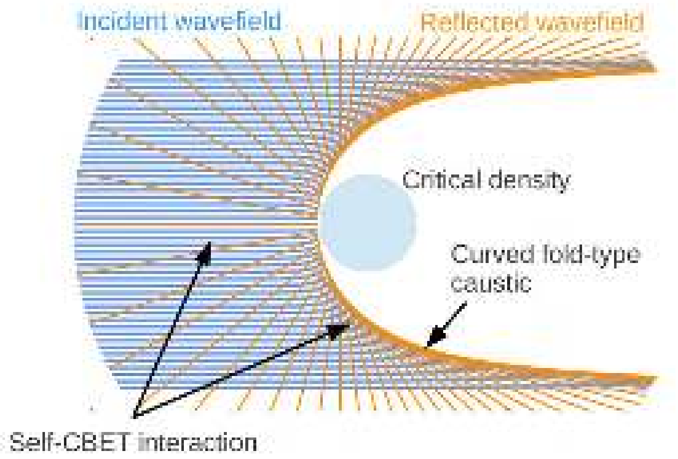

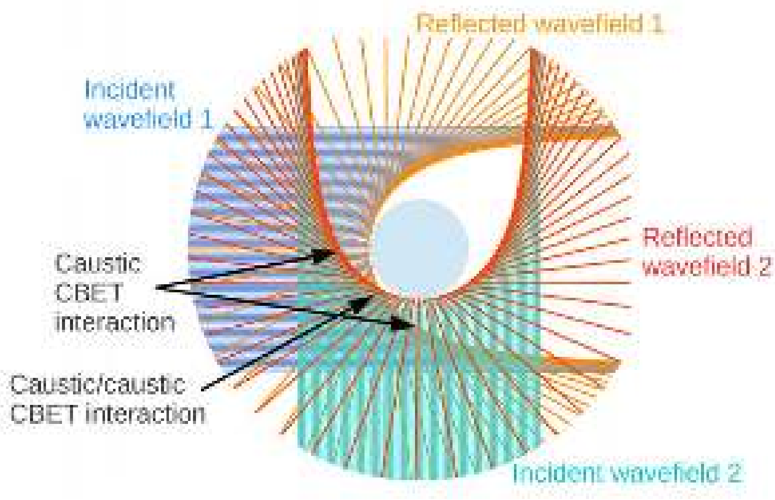

The number of CBET interaction coefficients to compute scales as $(4N_{beams}^2 - 2N_{beams})N_{cells}$
For polarized CBET with DPR smoothing, the scaling is $(64N_{beams}^2 - 8N_{beams})N_{cells}$

1- Introduction to inertial confinement fusion and a few typical degradation sources in implosions

2- Laser plasma transport and interaction modeling for study of low-mode degradations

3- Application to a study of “best-setup” OMEGA implosions

3.1 TWO CRYOGENIC SHOTS ARE CONSIDERED TO STUDY THE EFFECTS OF LOW MODES ON IMPLOSIONS

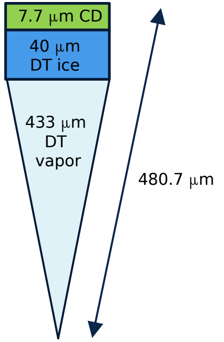

Cryo Shot 94712
Offset: ~ 7 µm*
Pointing: 7% mode l = 1
Measured hot-spot velocty: 146.3 km/s

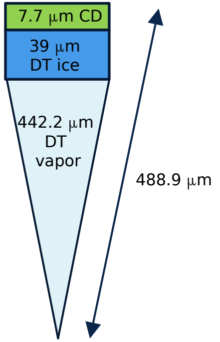

Cryo Shot 94343
Offset: 3.5 µm +/- 2.2 µm
Pointing: 1.7% mode l=1
Measured hot-spot velocity: 109.8 km/s

We study two cryo shots:
- shot 94712 with bad pointing
- shot 94343 with good pointing, low offset and low beam imbalance

Simulations are conducted with the ASTER/IFRIIT coupled code [A. Colaïtis, I. V. Igumenshchev et al. JCP (2021)]

*degraded data from 30s before shot with 45kg preload on the shroud

3.2 IN THE IDEAL CASE, ONLY PORT-INDUCED LOW MODES ARE PRESENT, EVENTUALLY MODIFIED BY CBET

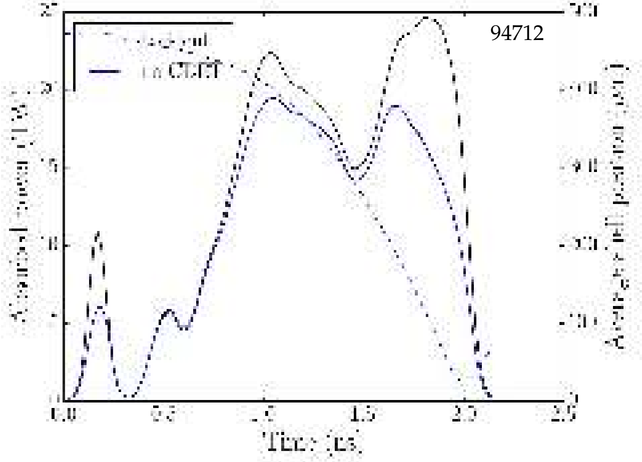

Mollweide projection of rho-r at stagnation

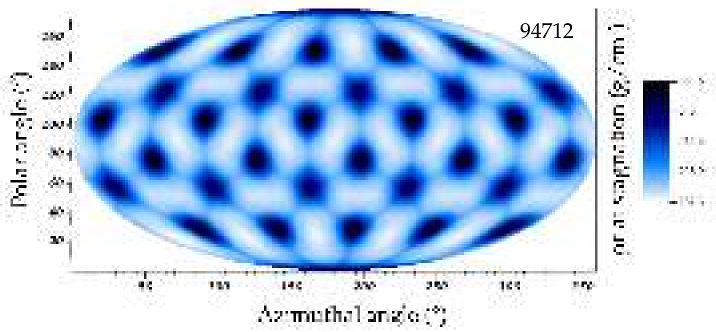

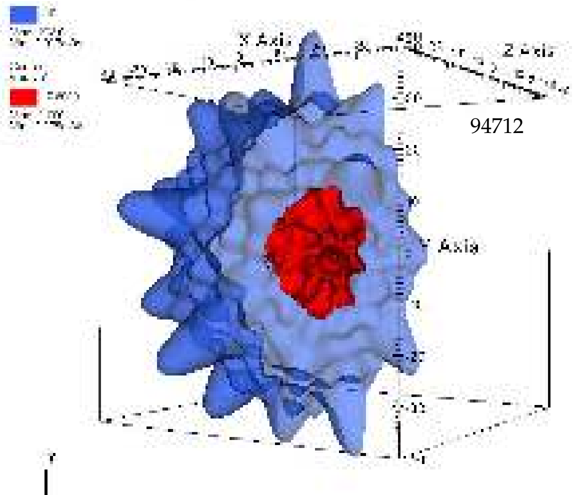

Ideal case: no mispointing, no offset, no imbalance

- no CBET: Yield ~ 1e15 neutrons

3.2 IN THE IDEAL CASE, ONLY PORT-INDUCED LOW MODES ARE PRESENT, EVENTUALLY MODIFIED BY CBET

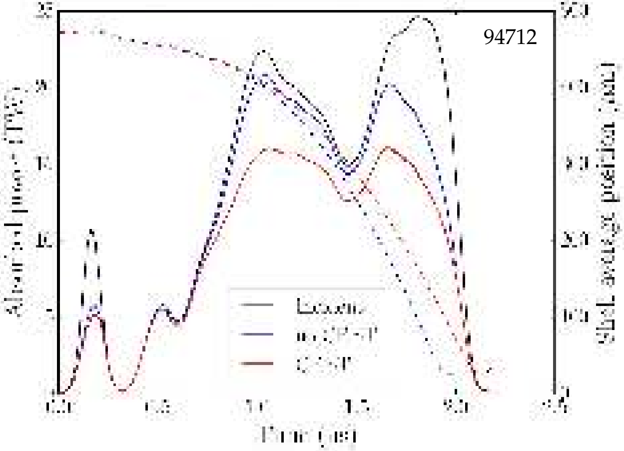

Ideal case: no mispointing, no offset, no imbalance

- no CBET: Yield ~ 1e15 neutrons
- CBET (unpolarized): 14.5% decrease in absorption
  Yield ~ 3.56e14 neutrons (35.6% YOC)

Mollweide projection of rho-r at stagnation

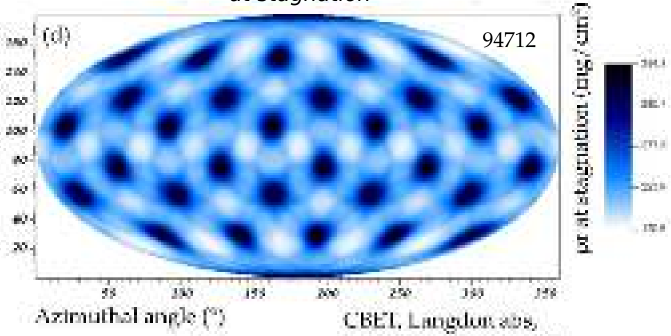

CBET, Langdon abs, dr/dt, Langdon CBET

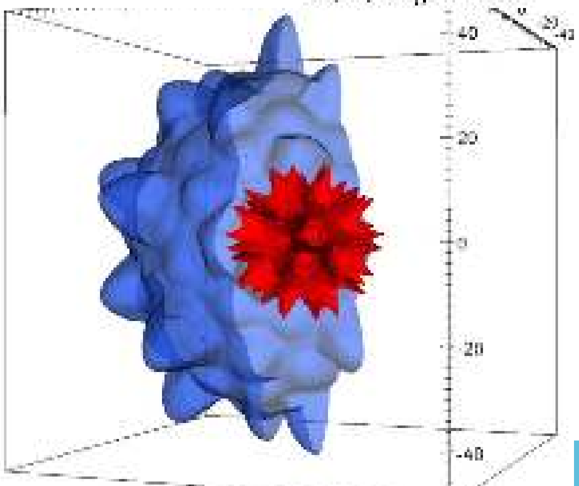

3.2 IN THE IDEAL CASE, ONLY PORT-INDUCED LOW MODES ARE PRESENT, EVENTUALLY MODIFIED BY CBET

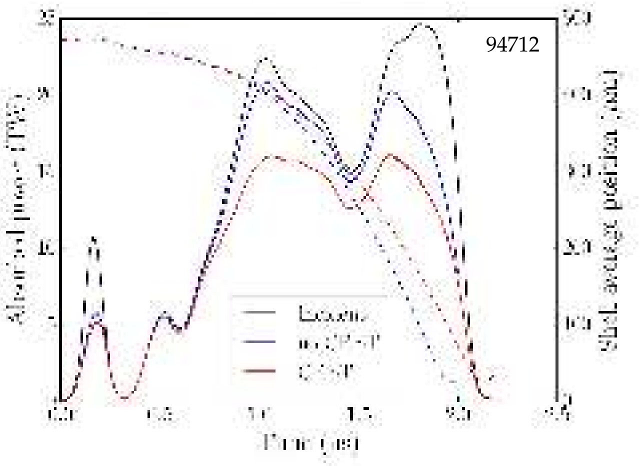

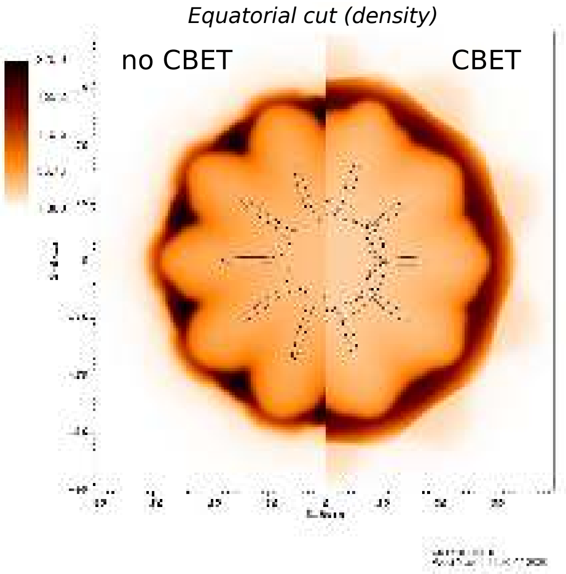

Ideal case: no mispointing, no offset, no imbalance

- no CBET: Yield ~ 1e15 neutrons
- CBET (unpolarized): 14.5% decrease in absorption
  Yield ~ 3.56e14 neutrons

3.3 OFFSET AND L=1 BEAM IMBALANCE HAVE SIMILAR NEFARIOUS EFFECT AND CAN LEAD TO SHELL BREAKUP

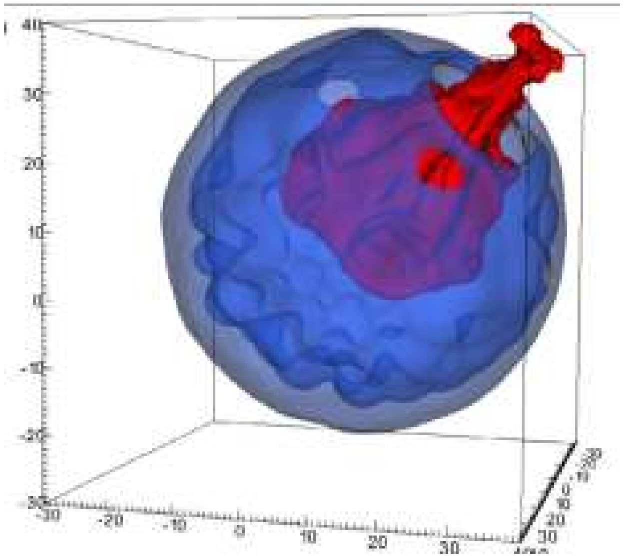

Effect of a 40 microns target offset

CBET Yield: 3.56e14 => 2.3e14

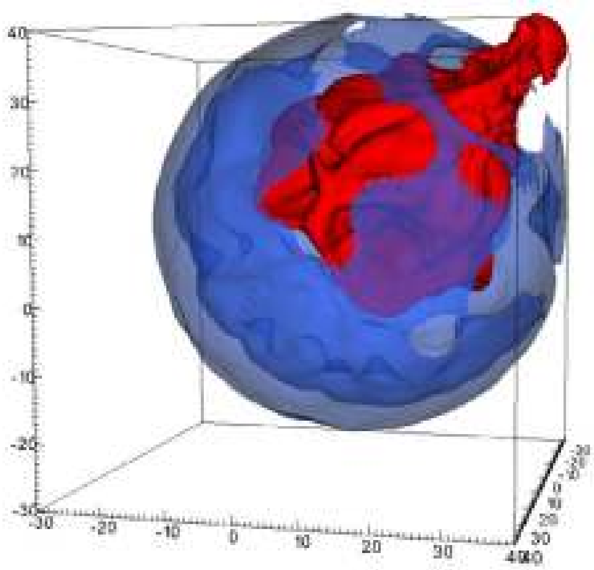

Effect of a 5% l=1 beam imbalance

CBET Yield: 3.56e14 => 1.5e14

3.4 WHILE CBET REDUCES YIELD, IT ALSO MITIGATES OFFSET AND IMBALANCE ERRORS

40 microns target offset; mitigation by CBET !

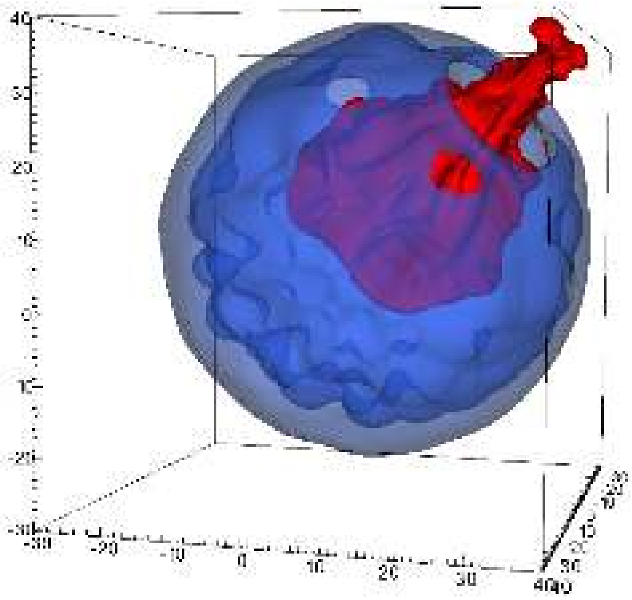

CBET Yield: 3.56e14 => 2.3e14

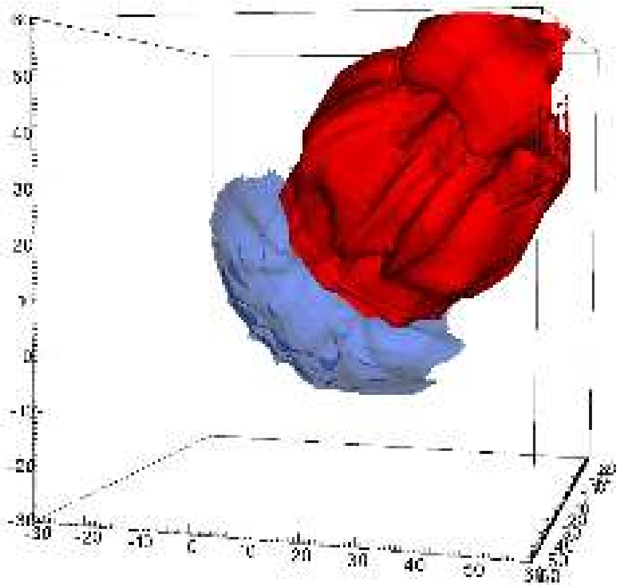

no CBET Yield: 1e15 => 6e13

The significant yield reduction without CBET is due to a completely broken shell

3.4 WHILE CBET REDUCES YIELD, IT ALSO MITIGATES OFFSET AND IMBALANCE ERRORS

5% beam balance error

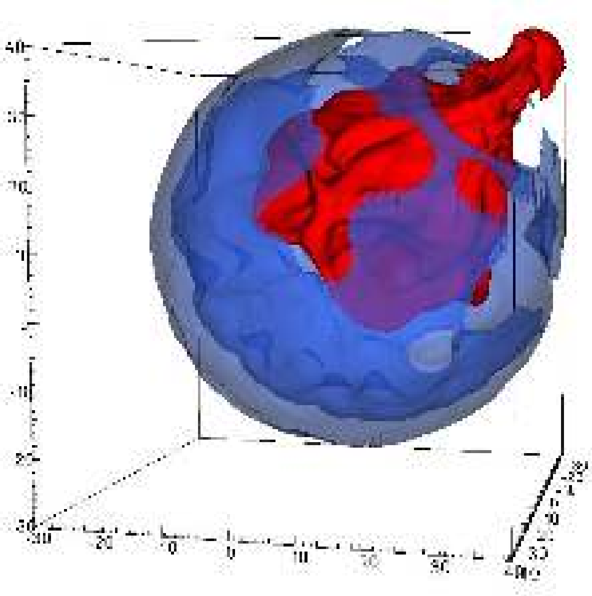

CBET Yield: 3.56e14 => 1.45e14

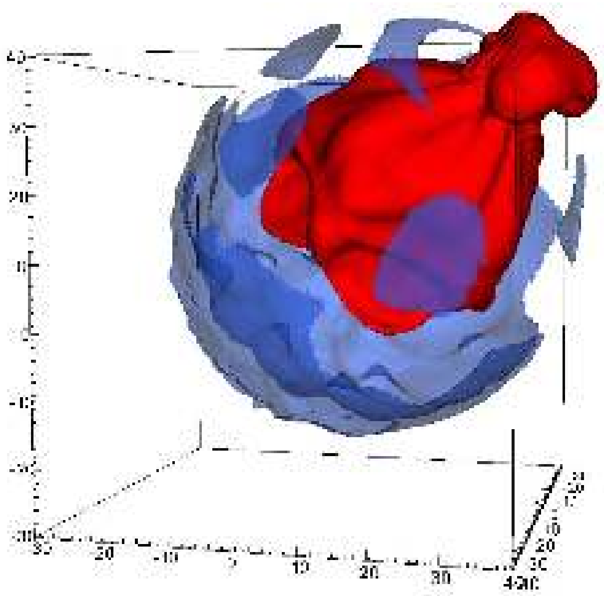

no CBET Yield: 1e15 => 2e14

Note that the yield increases but that is not significant; however the target is much more punctured

3.5 A DETAILED COMPARISON OF 94712 WITH DATA GIVES REASONABLE AGREEMENT WITH THE MODELING

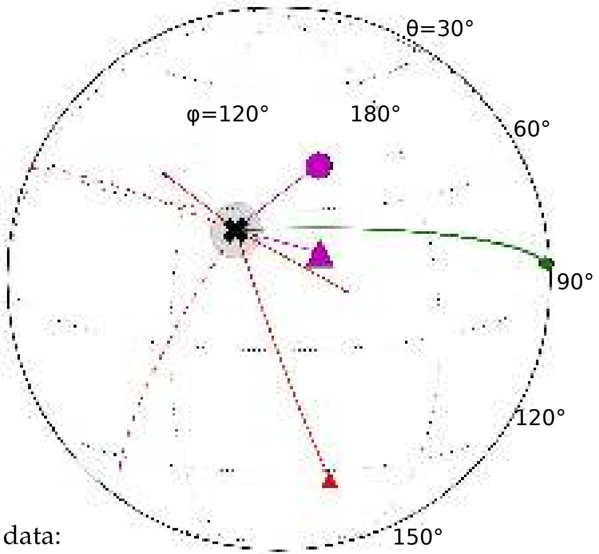

94712 data:
Offset: ~ 7 μm (not simulated for 94712)
Pointing: 7% mode l = 1

DT flow direction as measured from neutron data

Ideal balance and pointing
Real balance
Real balance and real pointing

o unpolarized CBET model
Δ polarized CBET model
⋆ no CBET

— with CBET
- - - without CBET

Symbol size ∝ flow velocity
Grey shade: error bar

- Angular anomaly dominated by **pointing**
- Closest point is polarized CBET with real balance and pointing (18° angular distance)
- Fuel aging (not modeled), is estimated to account for another 30% drop in yield
- Small-scale mixing may account for the remaining yield degradation

case	abs frac	peak neutron rise (ps)	yield (1e14) DT neutrons	l=1 areal mass mod. at stag. (microns)	final integrated flow velocity (km/s)	final integrated flow polar direction (°)	final integrated flow azimuthal direction (°)	Angular distance to measurement (°)
polarized CBET + DPR	71.1%	2107	1.51	4.28	168.2	69.4	152.9	18
data	N.A.	2081 +/- 50	0.77 +/- 0.054	N.A.	146.3 +/- 12	64.6 +/- 7	133.6 +/- 5	0

3.6 COMPARISON WITH 94343 HIGHLIGHTS THAT NOT ALL ASYMMETRY SOURCES HAVE YET BEEN UNDERSTOOD

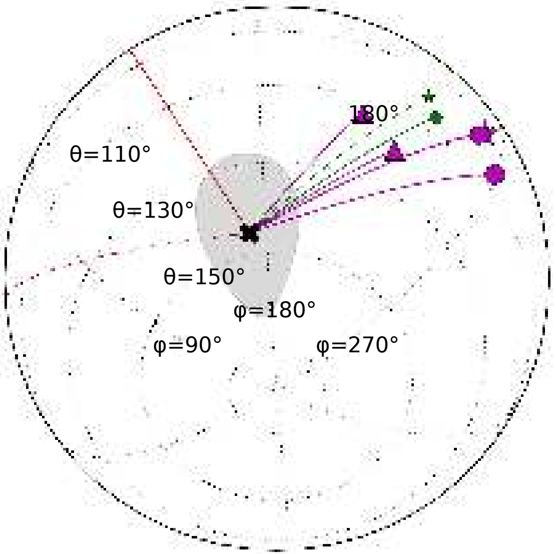

DT flow direction as measured from neutron data

Ideal balance and pointing
Real balance
Real balance and real pointing

o unpolarized CBET model
Δ polarized CBET model
⋆ no CBET

— with CBET
--- without CBET

Symbol size ∝ flow velocity
Grey shade: error bar

- Balance and pointing induce similar flow directions
- Both pointing and balance contribute to flow velocity (here constructively)
- Closest point is still the polarized CBET case with full input
- Potential culprits of the mismatch:
  - dynamic pointing derivation during shot day (can shift up to 90° at similar amplitude !)
  - stalk (although it is not clear if the systematic deviation changes between warm/cryo shots)

94343 data:
Offset: ~ 3.5 μm
Pointing: 1.7% mode l = 1

case	abs frac	peak neutron rise (ps)	yield (1e14) DT neutrons	l=1 areal mass mod. at stag. (microns)	final integrated flow velocity (km/s)	final integrated flow polar direction (°)	final integrated flow azimuthal direction (°)	Angular distance to measurement (°)
polarized CBET + DPR	73.5	2219	1.54	0.44	110.1	114	204.3	38
data	N.A. ?	2213 +/- 50	0.746 +/- 0.052	N.A.	109.8 +/- 15	145.3 +/- 18	174 +/- 18	0

CONCLUSION: SOME THOUGHTS ABOUT LOW MODES IN OMEGA ICF EXPERIMENTS

- Full scale modeling of ICF implosions is challenging in part due to micro-scale physics processes to be accounted for
- New modeling tools allow to probe better and better the interplay between these processes and the macroscopic (fluid) scale

---

- Even with **ideal pointing and balance**; polarized CBET can induce a flow up to 90 km/s (YOC=30%)
  => **mitigation of polarization effects are ultimately important**: need to redesign the OMEGA DPR system
- When all sources of imbalance are comparable and small, it seems like polarized CBET induces non-dominant effect over unpolarized CBET :
  => **mitigation of pointing and offset errors may be higher priority than mitigating polarization**
- **Decreasing pointing error from 7 to 1.7% does not change the yield** (in both the experiment and simulation) because the "low mode budget" of the implosion is quickly depleted !
- **Current best pointing (L=1 of 1.7%)/ low offset (3.5 microns) shots still have simulated YOC of 30% without CBET…**
  => we need to come up with direct-drive designs that are not so sensitive to such small errors.. !
  (low velocity schemes - shock ignition ? chambers with more beams ? different port configuration ? how does this change at ignition scale ?)

Backup slides

Inline Run 94712

	case	abs frac	peak neutron rise (ps)	yield (1e14) DT neutrons	l=1 areal mass mod. at stag. (microns)	final integrated flow velocity (km/s)	final integrated flow polar direction (°)	final integrated flow azimuthal direction (°)	Angular distance to measureme nt (°)
Ideal	nox_nodpr	86.9%	1932	9.8	0.01	0.5	147.8	355.3	136
Ideal	nox_dpr	86.6%	1935	10.	0.01	0.52	97.6	352.4	139
Ideal	x_unpol_nodpr	73.1%	2087	3.56	0.003	0.35	77.8	158.3	27
Ideal	x_unpol_dpr	72.3%	2102	3.58	0.02	1.18	54.0	112.5	21
Ideal	x_pol_dpr	71.6%	2110	3.02	1.97	86.9	122.8	156.6	62
Real Balance	x_unpol_nodpr	73.1%	2082	2.87	1.72	55.7	84.8	226.5	90
Real Balance	x_unpol_dpr	72.3%	2097	2.88	1.76	56.1	84.0	224.2	88
Real Balance Real Pointings	x_unpol_dpr	71.8%	2096	1.68	3.54	154.5	50.3	154.5	23
Real Balance Real Pointings	x_pol_dpr	71.1%	2107	1.51	4.28	168.2	69.4	152.9	18
	data	N.A. ?	2081* +/- 50	0.77 +/- 0.054	N.A.	146.3±12	64.6±7	133.6±5	0

*corrected for 61 ps time shift in ASTER/IFRIIT setup

Inline Run 94343

	case	abs frac	peak neutron rise (ps)	yield (1e14) DT neutrons	l=1 areal mass mod. at stag. (microns)	final integrated flow velocity (km/s)	final integrated flow polar direction (°)	final integrated flow azimuthal direction (°)	Angular distance to measurement (°)
Ideal	nox_dpr	86.8	2070	7.72	0.008	0.37	37.6	24.6	162
Ideal	x_unpol_dpr	74.4	2214	2.63	0.047	2.84	25.77	124	126
Real Balance	nox_dpr	86.8	2067	6.17	1.715	78.48	99.8	218.5	57
Real Balance	x_unpol_dpr	74.4	2209	2.1	1.174	53.7	104.9	221.2	54
Real Balance Real Pointings	nox_dpr	86.8	2062	3.41	3.33	171.6	96.4	234.4	68
Real Balance Real Pointings	x_unpol_dpr	74.3	2208	1.74	1.94	96.35	98.67	232.8	65
Real Balance Real Pointings	x_unpol_dpr_offset	74.1	2210	1.66	2.44	107	105	240	64
Real Balance Real Pointings	x_pol_dpr	73.5	2219	1.54	0.44	110.1	114	204.3	38
	x_pol_dpr_offset	73.5	2220	1.51	3.39	114	120	214	38
	data	N.A. ?	2213* +/- 50	0.746 +/- 0.052	N.A.	109.8±15	145.3±18	174±11	0

*corrected for 73 ps time shift in ASTER/IFRIIT setup